Iteration of B-spline surface based deflectometric method for discontinuous specular surface

Cheng Liu[1], Nan Gao[1], Zhaozong Meng[1], Zonghua Zhang[1,2 *], Feng Gao[2]

[1] School of Mechanical Engineering, Hebei University of Technology,

Tianjin 300401, China;

[2] EPSRC Advanced Metrology Hub, University of Huddersfield,

Huddersfield HD1 3DH, UK

*Correspondence: zhzhang@hebut.edu.cn

Abstract: There is an over-growing demand for accurate three-dimension model of industrial components. In the measurement of specular surface, deflectometry has been widely used for its convenience and high accuracy. However, it is a challenge to measure discontinuous specular surface by the traditional deflectometry. In order to solve this problem, this paper proposes a deflectometric method based on iteration of control points of B-spline surface. In this method, a screen at two positions displays fringe patterns reflected by specular surface under test and captured by a camera. According to the undistorted and absolute unwrapped phase map, a continuous zone containing all discontinuous area which is distinguished by a direct deflectometric method, is fitted by a B-spline surface with an estimated depth on the focus plane of the camera. Meanwhile, empty points and bridging control points are removed. The control points of the fitted surface are solved by iterative calculation. With the solved control points, discontinuous specular surface is reconstructed. Simulated and actual experiments are carried out and the results show high accuracy and stability of the proposed method.

Keywords: Deflectometry; Discontinuous specular surface; Iterative calculation; B-spline surface

1. Introduction

With the development of reverse engineering, manufacturing and et al, there is a growing demand for accurate reconstruction of every kind of components. The property of components' surface is generally classified into two categories: diffused surface and specular surface. The development of measurement of diffused surface has become mature [1-3], whereas the measurement of specular surface is still at an early stage. Components with specular surface are widely used in aerospace, automobile, optics system and artificial intelligence. Although interferometer is a superior technique reconstructing specular surface with high accuracy and resolution [4-6], the measurement needs expensive equipment. Phase measuring deflectometry (PMD) can effectively measures gradient and height of specular surface under test (SuT) and has advantages of full-field data acquisition, convenient equipment, non-contact operation, automatic data processing, high accurate data, and large dynamic range [7, 8].

In a system of PMD, there are usually a camera and a liquid crystal display (LCD). The relationship between the screen and the camera usually needs to be calibrated in advance. The LCD displays structured light patterns which is reflected by SuT and captured by the camera. The height and gradient of SuT are modulated in absolute phase extracted from the reflected patterns. Combined with known system parameters, the information of height and gradient can be extracted from the reflected maps.

Based on the principle of PMD, there are different methods to extract height and gradient information from the reflected absolute phase maps, such as iteration of gradient based PMD [9,10], light-tracking based PMD [11,12], model PMD(MPMD) [13,14], differential-geometry based PMD [15,16], direct PMD(DPMD) [17,18], stereoscopic PMD (stereo-PMD) [19]. The above methods are all good at reconstructing continuous specular surface. DPMD [17,18] directly formulates variation of phase and height, instead of integration of gradient. Light-tracking based PMD formulates incident ray and reflected ray to solve the reflected point. Thus, DPMD and light-tracking based PMD are also convenient to reconstruct discontinues or isolated specular surface. With excellent performance in

anti-noise, MPMD is good at reconstructing continuous specular surface in least square sense. Whereas, there is no clear discussion that MPMD reconstructs discontinuous specular surface.

In order to measure discontinuous specular surface with good resistance of noise, this paper proposes a deflectometric method based on iteration of B-spline surface. Firstly, this method conducts a geometric relationship to distinguish every isolated specular surface and obtain initial values of iteration. Then, with reprojection error on the screen as cost function, iteration proceeds to obtain control points of B-spline surface. Finally, SuT is constructed with the solved control points.

In the following, Section 2 explains the measuring principle of the proposed method. In Section 3, the simulated and actual experiments have been performed to verify the proposed method. Section 4 gives conclusion and future directions.

2. Principle

This section presents the principle of iteration of B-spline surface based deflectometric method for measuring discontinuous specular surface.

2.1 System configuration

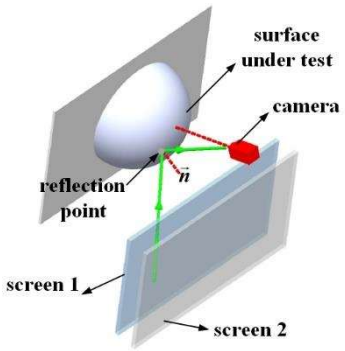

Fig. 1. Diagram of the PMD system.

The proposed method is performed in a deflectometric system, as shown in Fig.1. It contains a camera, and a screen which is fixed on a precise translating stage to locate two positions. In calibration of the system, geometric relationship between the camera and the screen at two positions needs to be calibrated, including a rotation matrix between the camera and the screen, two translation vectors between the camera and the screen at two positions. When a SuT is measured, the screen at two positions displays phase-shifted [20] horizontal and vertical sinusoidal fringes with fringe numbers N^2, N^2-1, N^2-N selected by the optimum fringe frequency method [21, 22]. At the two positions of the screen, the displayed fringes are reflected by the SuT, and then the fringe patterns are captured by the camera. As the fringes are undistorted and unwrapped, two pairs of absolute phase maps in two directions are obtained.

2.2 Reconstruction principle

The discontinuous specular surface is fitted by a B-spline surface. The control points of the fitted surface are solved by a procedure of iteration which reprojection error on the screen serves as a cost function.

2.2.1 Initial value of iteration

A direct deflectometric method, which based on the technique of DPMD and light tracking in PMD, is employed to obtain initial coordinate of SuT. With the reflected fringe patterns, the direct

method formulates coordinate of specular surface by geometry of inverse light. Thus, it is more convenient in initial value computation. With the initial coordinate, every isolated surface can be distinguished.

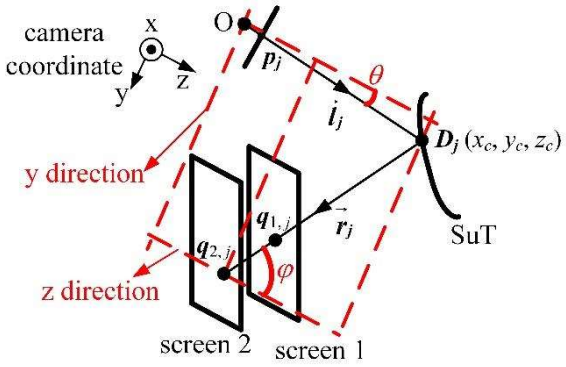

Fig. 2. Schematic diagram of the direct deflectometric method.

With the two pairs of undistorted absolute phase maps and results of calibration, the coordinate of SuT is computed in the camera coordinate system, as shown in Fig. 2. Among two pairs of phase maps, there are a number of a pixels in the camera corresponding to phase values. The jth pixel (j=1, …, a) corresponds to inverse incident light with direction $\vec{l}_j$ which can be computed by internal parameters of the camera. $\vec{r}_j$, which is the reflection of $\vec{l}_j$ by SuT at point $\boldsymbol{D}_j$, pass through points $\boldsymbol{B}_{i,j}$ (i=1, 2) on the screen at two positions whose coordinate are denoted as $\boldsymbol{q}_{i,j}$ which can be computed by geometric parameters of PMD. Along inverse light, there is a geometric relation on zoy plane of the camera coordinate

$$\boldsymbol{D}_j(z)\cdot\tan\theta+\left[\boldsymbol{D}_j(z)-\boldsymbol{q}_{2,j}(z)\right]\cdot\tan\varphi=\boldsymbol{q}_{2,j}(y) \tag{1}$$

where $\tan\theta$ is $\vec{l}_j(y)/\vec{l}_j(z)$ and $\tan\varphi$ is $-\vec{r}_j(y)/\vec{r}_j(z)$.

By extracting $\boldsymbol{D}_j$(z) in Eq. (1), z component of $\boldsymbol{D}_j$ can be computed by

$$\boldsymbol{D}_j(z)=\frac{\boldsymbol{q}_{2,j}(y)+\boldsymbol{q}_{2,j}(z)\tan\varphi}{\tan\theta+\tan\varphi} \tag{2}$$

As z component of $\boldsymbol{D}_j$ has been solved, x and y components of $\boldsymbol{D}_j$ can be solved by

$$\boldsymbol{D}_j(x,\ y)=\frac{\vec{l}_j(x,\ y)}{\vec{l}_j(z)}\cdot\boldsymbol{D}_j(z) \tag{3}$$

With total a pixels in the camera are computed by Eq. (1)- Eq. (3), SuT is reconstructed initially.

2.2.2 Procedure of iteration

In the two pairs of absolute phase map, a rectangular zone encircles all number of a pixels with known phase values. There are number of b pixels inside the rectangle and the rectangular zone needs to be modeled by the B-spline surface, as shown in Fig.3. Along $\vec{l}_j$, $\mathbf{D}_j(x_c, y_c, z_c)$ is captured by the jth (j=1, … , a) pixel $\mathbf{p}_j(x_f, y_f, f)$ on the virtual focus plane in front of the optical center, where f is the focus

length of the camera, as illustrated in Fig.4. $\mathbf{D}_j$ can be expressed as $s_j\mathbf{p}_j$ where s_j is a constant with value z_c/f.

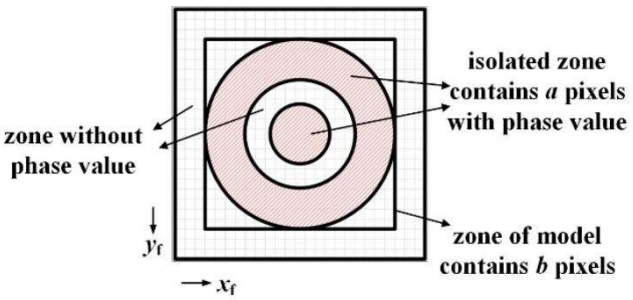

Fig. 3. An absolute phase map on the virtual focus plane undistorted and unwrapped from fringe patterns.

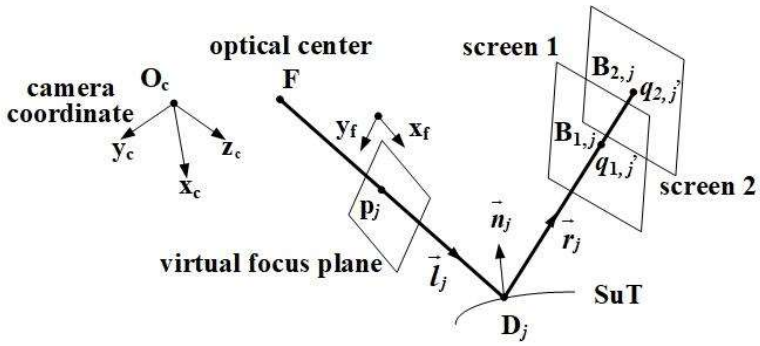

Fig. 4. Process of reprojection.

With an estimated depth z_{c0} of SuT which is average of $\boldsymbol{D}_j$ (z), a plane of s with values $\boldsymbol{x}_f$, $\boldsymbol{y}_f$, z_{c0}/f as x, y, z coordinates corresponding to every pixel inside the rectangle is fitted by a B-spline surface on the virtual focus plane in the form of

$$\boldsymbol{s} = \boldsymbol{W}\boldsymbol{P} \tag{4}$$

where $\boldsymbol{W}$ is a sparse matrix of basis functions, every row of $\boldsymbol{W}$ corresponds to a pixel inside the rectangle, every column of $\boldsymbol{W}$ corresponds to a control point, $\boldsymbol{P}$ is a column vector of control points, $\boldsymbol{s}$ is a column vector of s with b elements.

The gradients of the fitted plane in the direction of x_f and y_f are expressed as Eq. (5) and Eq. (6), respectively. Matrix $\boldsymbol{W}_x$ and $\boldsymbol{W}_y$ can be obtained by property of basis function.

$$\frac{\partial \boldsymbol{s}}{\partial \boldsymbol{x}_f} = \boldsymbol{W}_x \boldsymbol{P} \tag{5}$$

$$\frac{\partial \boldsymbol{s}}{\partial \boldsymbol{y}_f} = \boldsymbol{W}_y \boldsymbol{P} \tag{6}$$

Although B-spline basis function has excellent local properties, the fitting error is large near to edge of discontinuous surface. Thus, it is necessary to abandon the basis functions and corresponding control points which bridge isolated surface. Because there are pixels inside the rectangle without phase values and there are basis functions bridge isolated surface which are judged by $\boldsymbol{D}_j$ (z), rows and columns of $\boldsymbol{W}$, $\boldsymbol{W}_x$ and $\boldsymbol{W}_y$ corresponding to these pixels and those control points need to be abandoned to keep $\boldsymbol{W}$ full-column rank [23] to avoid ill-condition matrixes in iteration.

As initial value s, $\frac{\partial s}{\partial x_f}$ and $\frac{\partial s}{\partial y_f}$ have been obtained. The fitted plane of s on the virtual focus plane needs to be transformed to the camera coordinate. The relationship between gradients on the virtual focus plane and on the camera coordinate can be expressed as the following equations

$$\begin{aligned}&\frac{\partial z_c}{\partial x_f} = \mathrm{f}\cdot\frac{\partial s}{\partial x_f} = \\ &\frac{\partial z_c}{\partial x_c}\frac{\partial x_c}{\partial x_f}+\frac{\partial z_c}{\partial y_c}\frac{\partial y_c}{\partial x_f} = \frac{\partial z_c}{\partial x_c}\left(x_f\frac{\partial s}{\partial x_f}+s\right)+\frac{\partial z_c}{\partial y_c}\left(y_f\frac{\partial s}{\partial x_f}\right)\end{aligned} \tag{7}$$

$$\begin{aligned}&\frac{\partial z_c}{\partial y_f} = \mathrm{f}\cdot\frac{\partial s}{\partial y_f} = \\ &\frac{\partial z_c}{\partial x_c}\frac{\partial x_c}{\partial y_f}+\frac{\partial z_c}{\partial y_c}\frac{\partial y_c}{\partial y_f} = \frac{\partial z_c}{\partial x_c}\left(x_f\frac{\partial s}{\partial y_f}\right)+\frac{\partial z_c}{\partial y_c}\left(y_f\frac{\partial s}{\partial y_f}+s\right)\end{aligned} \tag{8}$$

Combine Eq. (7) and Eq. (8), the gradients of the initial plane on the camera coordinate $\frac{\partial z_c}{\partial x_c}$ and $\frac{\partial z_c}{\partial y_c}$ can be extracted. The normal direction $\vec{n}$ of SuT on the camera coordinate can be computed by $\frac{\partial z_c}{\partial x_c}$ and $\frac{\partial z_c}{\partial y_c}$. Reflected by SuT, the inverse light $\vec{l}_j$ from the jth pixel of the camera intersects the ith screens at point $\mathbf{B}_{i,\,j}$ (i=1, 2) along light path $\vec{r}_j$ which can be expressed as $\frac{2\left(\vec{l}_j\cdot\vec{n}_j\right)\vec{n}_j}{\left\|\vec{n}_j\right\|^2\left\|\vec{l}_j\right\|}-\frac{\vec{l}_j}{\left\|\vec{l}_j\right\|}$. With geometric parameters of PMD, the coordinates of point $\mathbf{B}_{i,\,j}$ can be computed which are denoted as $\boldsymbol{q}_{i,\,j}'(\boldsymbol{P})$. With $\boldsymbol{P}$ as arguments and norm of reprojection error as dependent, the cost function $g(\boldsymbol{P})$ is set up in Eq. (9). The solved $\boldsymbol{P}$ is obtained to minimize Eq. (9) by the Gauss–Newton method (GN) or the Levenberg-Marquardt method (LM) [24].

$$g\left(\boldsymbol{P}\right)=\sum_{i=1}^{2}\sum_{j=1}^{a}\left\|\boldsymbol{q}_{i,j}'\left(\boldsymbol{P}\right)-\boldsymbol{q}_{i,j}\right\|^2 \tag{9}$$

With the solved $\boldsymbol{P}$, the coordinate of the measured specular surface can be expressed as f($\boldsymbol{WP}$).*$\mathbf{p}$, where $\mathbf{p}$ is [$\mathbf{p}_1$; $\mathbf{p}_2$; …; $\mathbf{p}_a$], where '.*' denotes Hadamard product after f($\boldsymbol{WP}$) expended to the same dimension with $\mathbf{p}$.

3. Experiments

3.1 Simulated experiments

For testing the proposed deflectometric method, some simulation experiments have been carried out. Two positions of a plane screen and a camera are placed as shown in Fig. 1. A right-handed world coordinate's xoy plane was fixed on a reference plane. Screen at two positions was parallel to the reference plane with distance 100 mm and 130 mm. The pixel coordinate system on the screen is parallel to x, y axis of the world coordinate. Rotation matrix and translation vector between the camera and the reference plane are $\begin{pmatrix} 0.9976 & 0 & 0.0698 \\ 0.0061 & 0.9962 & -0.0869 \\ -0.0695 & 0.0872 & 0.9938 \end{pmatrix}$ and $\begin{pmatrix} 0 \\ 0 \\ 402.5084 \end{pmatrix}$, respectively. The deflectometric system is illustrated in Fig.5. A discontinuous specular step, as illustrated in Fig. 6. (a), is expressed as the following equation in the world coordinate system.

$$z=\begin{cases} -25\ , \sqrt{x^2+(y+5)^2} \le 4 \\ -15\ ,\ 5.5 \le \sqrt{x^2+(y+5)^2} \le 10 \\ 0\ ,\ 11.5 \le \sqrt{x^2+(y+5)^2} \le 16 \end{cases} \tag{10}$$

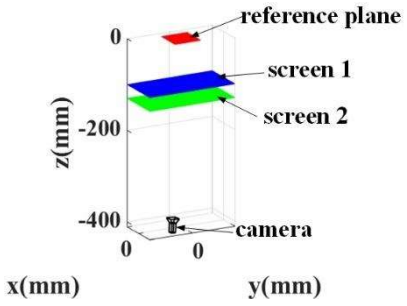

Fig. 5. Diagram of simulated system.

Noises with different levels were added into the generated fringe patterns by

$$I_{noisy}=I_{ideal}\cdot(1+i\cdot 0.2/100\cdot randn) \tag{11}$$

where I_{noisy} denotes the generated noisy fringe pattern, i is the noise level and i=0, …, 15, *randn* is a matrix whose element obeys standard normal distribution. The generated fringe patterns at two positions of the screen are given in Fig.6 (b) and (c).

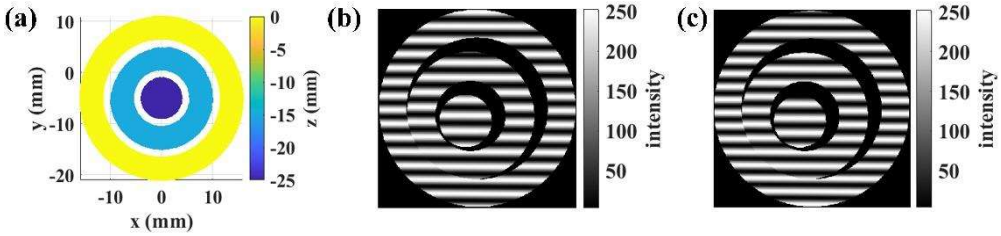

Fig. 6. Specular step and generated fringe patterns. (a) Specular step in the world coordinate; (b), (c) one of the generated fringe patterns at positions of the screen 1 and screen 2.

At different noise levels, the measured coordinates of every surface were fitted to a plane. The root mean square (RMS) distance between the points of the adjacent surface and the fitting plane was treated as the measured distance. With an estimated depth z_{c0}=380 mm, distance errors of the

reconstructed specular step at different noise levels are illustrated in Fig. 7. At noise level i=10, the process of iteration and distribution of reprojection error on the screen at two positions with solved $\boldsymbol{P}$ are illustrated in Fig. 8.

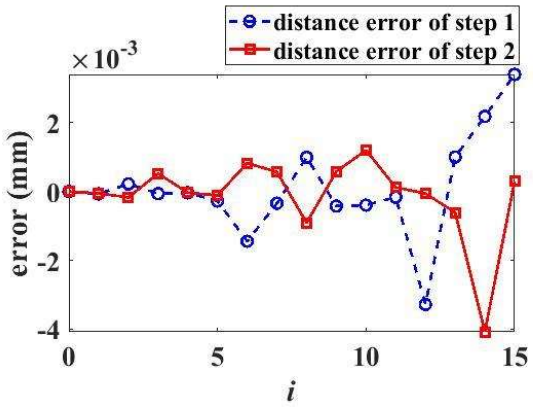

Fig. 7. Distance error at different noise levels.

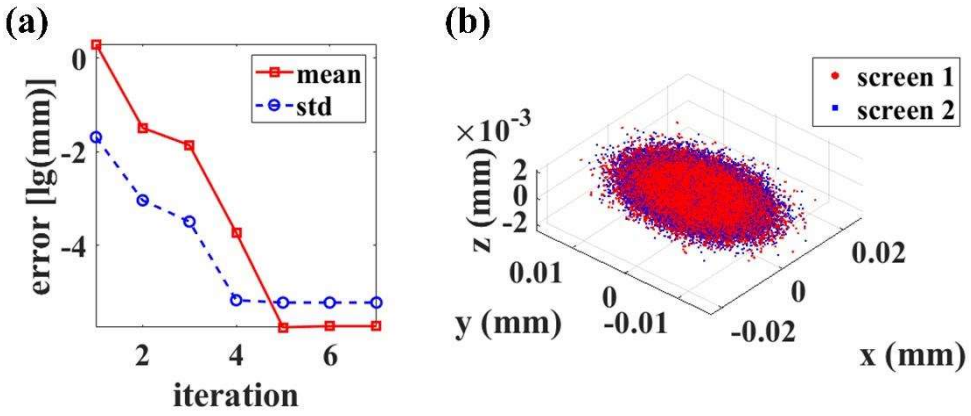

Fig. 8. Process of iteration and distribution of error with solved P when i=10. (a) The mean reprojection error and its standard deviation, (b) distribution of reprojection error on two positions of the screen.

The simulated experimental results indicate that the proposed deflectometric method is of high noise resistance and high reconstruction accuracy.

3.2 Actual experiments

3.2.1 Hardware of the deflectometry system

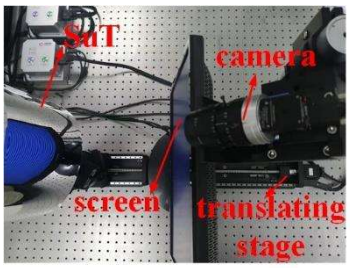

Fig. 9. Hardware diagram of stereo-PMD system.

The deflectometric system consists of a plane screen, a camera, and a translating stage, as depicted in Fig. 9. The screen is fixed on the translating stage. The cameras (XIMEADE XIQ, MQ042CG-CM, Germany) have a resolution of 2048 × 2048 pixels, and use a standard prime lens

(AZURE-1620ML5M) of focal length 16 mm. The model of the plane screen is ENVISION H925W, with a resolution of 1440*900, pixel size of 0.283 mm*0.283 mm. The translating stage (DHC, GCD-20Series, Beijing, China) has an accuracy of 1 μm.

3.2.2 System calibration

Calibration of the PMD system is to confirm geometric relationship between the camera and the screen at two positions. The screen at two positions displayed checker pattern with every grid 45 *45 pixel. At position one of the screen, a flat mirror with twenty-one different poses was used to reflect the displayed checker pattern. The accuracy of calibration depends on the accuracy of corners extraction. Thus, the camera focused on virtual images of the checker pattern. Twenty-one reflected checker patterns were recorded and featured points were extracted. With the extracted feature points, the system was calibrated to obtain the intrinsic parameters of the camera, the rotation matrix and the translation vector between the camera and the screen at position 1[25, 26]. At the last orientation of the flat mirror, the screen was translated by the translating stage to the position 2 and the camera recorded the reflected checker pattern. With the obtained intrinsic parameters of the camera and the rotation matrix, the featured points were extracted and the translation vector between the camera and the screen at position 2 was computed with the minimum reprojection error [27]. The distribution of reprojection error on the camera at the position 1, the extracted and reprojected feature points at the position 2 are illustrated in Fig. 10. Standard deviation (STD) of reprojection error on camera are [0.0434, 0.0383] pixel and [0.0516, 0.0444] pixel, respectively, at the two positions. The calibrated PMD system in the camera coordinate is illustrated in Fig. 11.

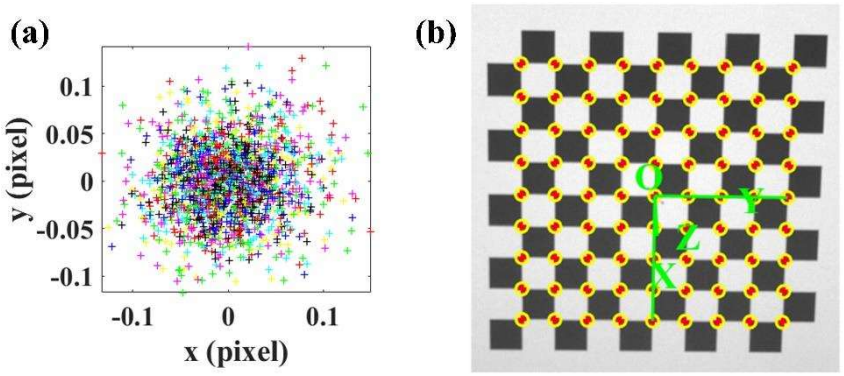

Fig. 10. Reprojection of the featured points. (a) distribution of reprojection error at position 1; (b) extracted and reprojected featured points at position 2 where '+' and '〇' denote extracted and reprojected featured points respectively.

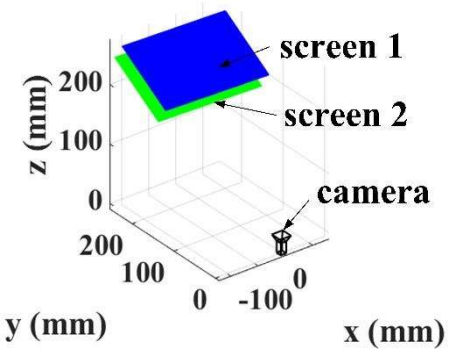

Fig. 11. Calibrated PMD system in the camera coordinate.

3.2.3 Experiments on specular surface

In order to evaluate the proposed deflectometric method, the PMD system measured a specular step, a specular monolithic multi-surfaces workpieces (MMSWs) and isolated parts of a flat mirror, as illustrated in Fig. 12. As the screen displayed vertical and horizonal fringe patterns, the camera focused on a position where virtual images reflected by isolated specular surface can be clearly captured simultaneously and then reflected fringe patterns were recorded. Several recorded fringe patterns are illustrated in Fig. 13. (a)-(c) and corresponding absolute phase maps are illustrated in Fig. 13. (d)-(f).

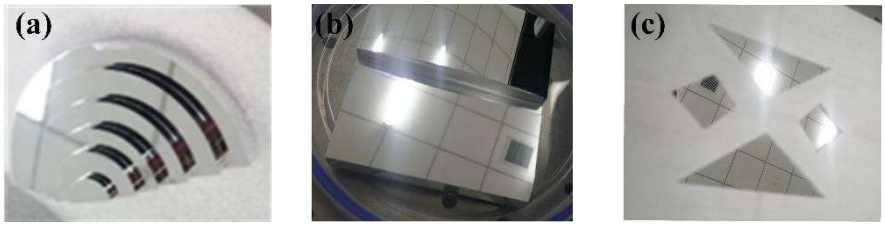

Fig. 12. Surface under test. (a) Specular step; (b) Specular monolithic multi-surfaces workpieces; (c) Isolated parts of a flat mirror.

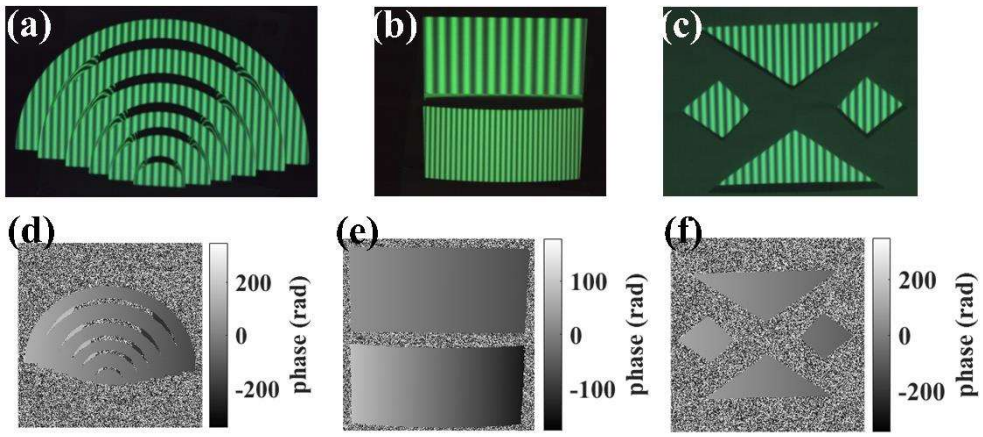

Fig. 13. Reflected fringe patterns by SuT. (a)-(c) Reflected fringe patterns at a position of screen by specular step, MMSWs and isolated parts of a flat mirror, respectively; (c)-(d) Absolute phase maps of specular step, MMSWs and isolated parts of a flat mirror, respectively.

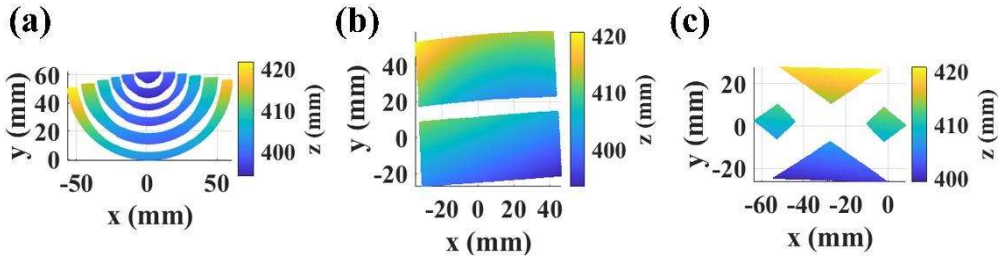

Fig. 14. Initial reconstruction of SuT by direct deflectometric method. (a)-(c) Initial reconstruction of specular step, MMSWs and isolated parts of a flat mirror, respectively.

With the absolute phase maps and the calibrated parameters, the real position $\boldsymbol{q}_{i,j}$ can be obtained. The direct deflectometric method in Section 2.2.1 was conducted to reconstruct SuT initially, as illustrated in Fig. 14. With average values of initial reconstruction, $\boldsymbol{W}$, $\boldsymbol{W}_x$, $\boldsymbol{W}_y$ and initial $\boldsymbol{P}$ were computed. The cost functions of different SuT in the form of Eq. (9) were minimized iteratively to get

P. As iterations proceed, pixels which correspond to large reprojection error were abandoned. The process of iteration, distribution of reprojection error on the screen with the solved ***P*** and reconstruction of SuT by proposed method are illustrated in Fig. 15.

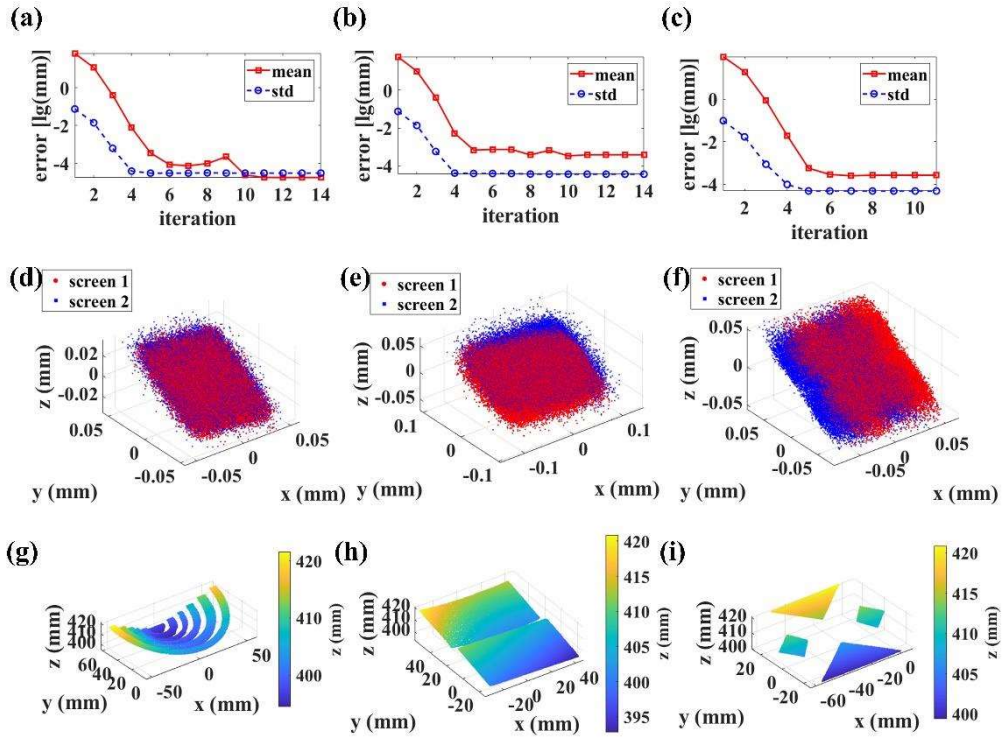

Fig. 15. Process of iterations, distribution of reprojection error on the screen and reconstruction of SuT by proposed method. (a)-(c) Process of iterations of specular step, MMSWs and isolated parts of a flat mirror, respectively. (d)-(f) Reprojection error with solved control points of specular step, MMSWs and isolated parts of a flat mirror, respectively. (g)-(h) Reconstruction of specular step, MMSWs and isolated parts of a flat mirror by proposed method, respectively.

Table 1. Actual distance, measurement distance of step and error (mm)

	actual distance	measured distance	absolute error
step1~2	6.5000	6.5122	0.0122
step2~3	5.5000	5.5121	0.0121
step3~4	5.0000	4.9996	-0.0004
step4~5	4.0000	4.0018	0.0018
step5~6	3.0000	2.9972	-0.0028

The actual distance between steps of specular step was measured by a C32-bit ZEISS Calypso coordinate measuring machine, as shown in Table 1. The measured coordinates of every surface were fitted to a plane. The distance between the points of the adjacent step and the fitting plane was treated as the measured distance. Table 1 shows the comparisons between the actual distance and the measured distance. Furthermore, the root mean square error (rmse) between the fitted planes and coordinate of every step reconstructed by the proposed iterative method are in the range of 10^{-4}-10^{-5} mm which is lower than initial reconstruction with rmse in level of 10^{-2} mm. With the reconstruction of the isolated part of a flat mirror, the rmse between the fitted plane and reconstructed coordinate is 0.0240 mm for

proposed iterative method, whereas 0.0879 mm for initial reconstruction. Therefore, the proposed iterative method is more resistant to noise.

The cylindrical part of MMSWs is designed with a radius of 210 mm which serves as a representation of curved specular surface in discontinuous specular components. The distance between plane part of MMSWs and axis of cylindrical part is 201.1533 mm. With the reconstruction by the proposed iterative method, a cylinder with radio of 209.9950 mm is fitted to cylindrical part with rmse $4.5345*10^{-4}$ mm, in least square sense; A plane is fitted to plane part with rmse 0.0015 mm. The lines between every sample point on the plane part and a point on the axis have average projection length 201.1953 mm in the normal direction of the fitted plane. Distribution of distance between fitted surface and reconstruction is illustrated in Fig. 16.

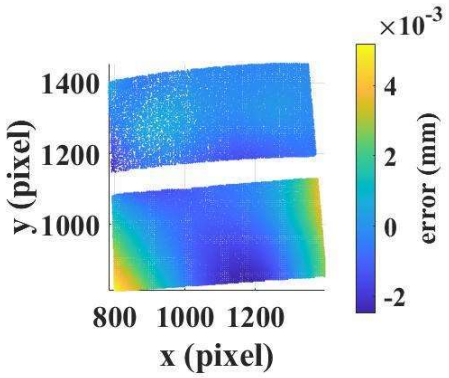

Fig. 16. Distance between reconstruction and fitted surface.

The results indicate that reconstruction of the discontinuous specular surface by the proposed deflectometric method has high accuracy.

4. Conclusion

In this paper, a deflectometric method based on iteration of B-spline surface has been proposed to measure discontinuous specular surface. A screen displaying fringe patterns locates at two positions by a translating stage. With an estimated depth, the discontinuous surface under test is modeled by a B-spline surface. Different from a global defined model, such as Bezier surface, the local defined B-spline is good at reconstructing discontinuous surface. With the procedure of iteration, the proposed method reconstructs specular surface in least square sense, so it is very robust to noise. The principle of the proposed method is minimizing a cost function of reprojection error iteratively to compute control points of the modeled surface. With estimated initial values for iteration of the different discontinuous specular components, simulated and actual experiments show high accuracy and stability of the proposed method. In the future, more accurate calibration methods and iteration with higher efficiency will be furtherly studied.

Funding

The authors wish to acknowledge the support by the National Natural Science Foundation of China (under Grant No. 52075147, 51675160).

References

[1] Zhang Z H. Review of single-shot 3D shape measurement by phase calculation-based fringe projection techniques. Opt. Lasers Eng. 2012; 50(8): 1097-1106.

[2] Zhang S. Recent progresses on real-time 3D shape measurement using digital fringe projection techniques. Opt. Lasers Eng. 2010; 48: 149-158.

[3] Zuo C, Chen Q, Gu G H, et al. High-speed three-dimensional profilometry for multiple objects with complex shapes. Opt. Express. 2012; 20: 19493-19510.

[4] Wyant J. White light interferometry. Proc. SPIE. 2002; 4737: 98-107.

[5] Jiang X Q, Wang K, Gao F, et al. Fast surface measurement using wavelength scanning interferometry with compensation of environmental noise. Appl. Opt. 2010; 49: 2903-2909.

[6] Dávila A. Wavelength scanning interferometry using multiple light sources. Opt. Express. 2016; 24: 5311-5322.

[7] Bothe T, Li W S, Kopylow C V, et al. High-resolution 3D shape measurement on specular surfaces by fringe reflection. Proc. SPIE. 2004; 5457: 411-422.

[8] Zhang Z H, Wang Y M, Huang S J, et al. Three-Dimensional shape measurements of specular objects using phase-measuring deflectometry. Sensors 2017; 17(12): 2835.

[9] Tang Y, Su X Y, Liu Y K, et al. 3D shape measurement of the aspheric mirror by advanced phase measuring deflectometry. Opt. Express. 2008; 16: 15090-15096.

[10] Tang Y, Su X Y, Wu F, et al. A novel phase measuring deflectometry for aspheric mirror test," Opt. Express. 2009; 17: 19778-19784.

[11] Guo H W, Tao T. Specular surface measurement by using a moving diffusive structured light source. Proc. SPIE. 2007; 6834: 68343E.

[12] Guo H W, Feng P, Tao T. Specular surface measurement by using least squares light tracking technique. Opt. Laser Eng. 2010; 48: 166-171.

[13] Huang L, Xue J P, Gao B, et al. Modal phase measuring deflectometry. Opt. Express. 2016; 24(21): 24649-24664.

[14] Huang L, Xue J P, Gao B, et al. Three-dimensional shape measurement with modal phase measuring deflectometry. Proc. SPIE. 2017; 1044909: 1-10.

[15] Liu M M, Hartley R, Salzmann M. Mirror surface reconstruction from a single image. IEEE Trans. Pattern Anal. Mach. Intell. 2015; 37(4): 760-773.

[16] Tarini M, Lensch H P A, Goesele M, et al. 3D acquisition of mirroring objects using striped patterns. Graph. Models 2005; 27(4): 223-259.

[17] Liu Y, Huang S J, Zhang Z H, et al. Full-field 3D shape measurement of discontinuous specular objects by direct phase measuring deflectometry. Sci. Rep. 2017; 7: 10293.

[18] Zhao P, Gao N., Zhang Z H, et al. Performance analysis and evaluation of direct phase measuring deflectometry. Opt. Lasers Eng. 2018; 103: 24-33.

[19] Knauer M C, Kaminski J, Hausler G. Phase measuring deflectometry: a new approach to measure specular free-form surfaces. Proc. SPIE. 2004; 5457: 336-376.

[20] Srinivasan V, Liu H C, Halioua M. Automated phase-measuring profilometry of 3-D diffuse objects. Appl. Opt. 1984; 23: 3105-3108.

[21] Zhang Z H, Towers C E, Towers D P. Time efficient color fringe projection system for 3D shape and color using optimum 3-frequency Selection. Opt. Express. 2006; 14: 6444-6455.

[22] Towers C E, Towers D P, Jones J D C. Generalized frequency selection in multifrequency interferometry. Opt. Lett. 2004; 29(12): 1348-1350.

[23] Liu C, Gao N, Meng Z Z, et al. B-spline surface based 3D reconstruction method for

deflectometry. Opt. Express. 2022; 30: 28207-28219.

[24] Madsen K, Nielsen H B, Tingleff O. Methods for non-linear least squares problems. 2th ed. Informatics and mathematical modelling technical university of Denmark; 2004.

[25] Xiao Y L, Li S K, Zhang Q C, et al. Optical fringe-reflection deflectometry with bundle adjustment. Opt. Lasers Eng. 2018; 105: 132-140.

[26] Xiao Y L, Su X Y, Chen W J. Flexible geometrical calibration for fringe-reflection3D measurement. Opt. Lett. 2012; 37(4): 620-622.

[27] Zhang Z Y. A flexible new technique for camera calibration. IEEE Trans. Pattern Anal. Mach. Intell. 2000; 22(11): 1330-1334.